Available online at www.sciencedirect.com
SCIENCE DIRECT®
Inorganica Chimica Acta 358 (2005) 2629–2642
Inorganica Chimica Acta
www.elsevier.com/locate/ica

Study of the spectroscopic and electrochemical properties of tetraruthenated porphyrins by theoretical–experimental approach

Ildemar Mayer [a], André L.B. Formiga [a], Fábio M. Engelmann [a], Herbert Winnischofer [a], Pedro V. Oliveira [a], Daniela M. Tomazela [b], Marcos N. Eberlin [b], Henrique E. Toma [a], Koiti Araki [a,*]

[a] *Instituto de Química, Universidade de São Paulo, C. Postal 26077, CEP 05513-970 São Paulo (SP), Brazil*
[b] *Thomson Mass Spectrometry Laboratory, Institute of Chemistry, State University of Campinas, UNICAMP, Campinas SP 13083-970, Brazil*

Received 9 September 2004; accepted 6 March 2005
Available online 18 April 2005

Abstract

The spectroscopic and electrochemical properties of two isomeric forms of the supramolecular species $[\mu\text{-}(H_2TPyP)\{Ru(bpy)_2Cl\}_4]^{4+}$ (H_2TPyP = 5,10,15,20-tetra(3- or 4-pyridyl)porphyrin, bpy = 2,2′-bipyridine) have been compared and consistently interpreted with the aid of molecular orbital calculations. In these complexes, the HOMO and LUMO levels are predominantly localized in the ruthenium complexes and porphyrin ring, respectively. There is an extensive mixing of the wave functions of both components in other MOs, however, and their contributions are reflected in the spectroelectrochemical and spectroscopic behavior. For example, the electronic mixing is enough to allow the energy-transfer from the peripheral complexes to the porphyrin ring, as well as the appearance of a $Ru^{II}(d\pi) \rightarrow H_4P(p\pi^*)$ charge-transfer band at 700 nm in the bis-protonated $[\mu\text{-}(H_4TPyP)\{Ru(bpy)_2Cl\}_4]^{4+}$ species, showing the strong stabilization of the porphyrin LUMO levels.

Keywords: Supramolecular porphyrins; Ruthenium polypyridines; Spectroscopy; Electrochemistry; Photophysics; Molecular mechanics

1. Introduction

In the last decade, many efforts have been focused on the preparation of sophisticated molecules by assembling smaller units through covalent bonds and even weak molecular interactions [1]. Such molecular building blocks can be specially chosen in order to impart their photochemical, catalytic, electrocatalytic and electron-transfer properties to the supramolecular systems [2–19]. A fine-tuning of their electronic properties is also required to optimize the cooperative interactions between the several components. This relevant subject, which can be further exploited in supramolecular chemistry, requires a careful investigation since it can be influenced by subtle interactions, not always possible to be evaluated without suitable systems for comparison. Fortunately, the theoretical methods have evolved extraordinarily in the last decade, constituting a worthy tool for the study and interpretation of molecular and supramolecular properties [20–29].

Supramolecular porphyrins obtained by the coordination of $[Ru(bpy)_2Cl]^+$ complexes [30,31] (where bpy = 2,2′-bipyridine) and $[Ru_3O(OAc)_6(py)_2]^+$ trinuclear ruthenium acetate clusters [19,32] (where py = pyridine and OAc = acetate) to the pyridyl N-atoms of *meso*-tetra(4-pyridyl)porphyrins, M(4-TPyP), have been systematically investigated in our laboratory in recent years. This approach has allowed us to combine the

* Corresponding author. Tel.: +55 11 3091 3887; fax: +55 11 3815 5579.
E-mail address: koiaraki@iq.usp.br (K. Araki).

0020-1693/$ - see front matter © 2005 Elsevier B.V. All rights reserved.
doi:10.1016/j.ica.2005.03.020

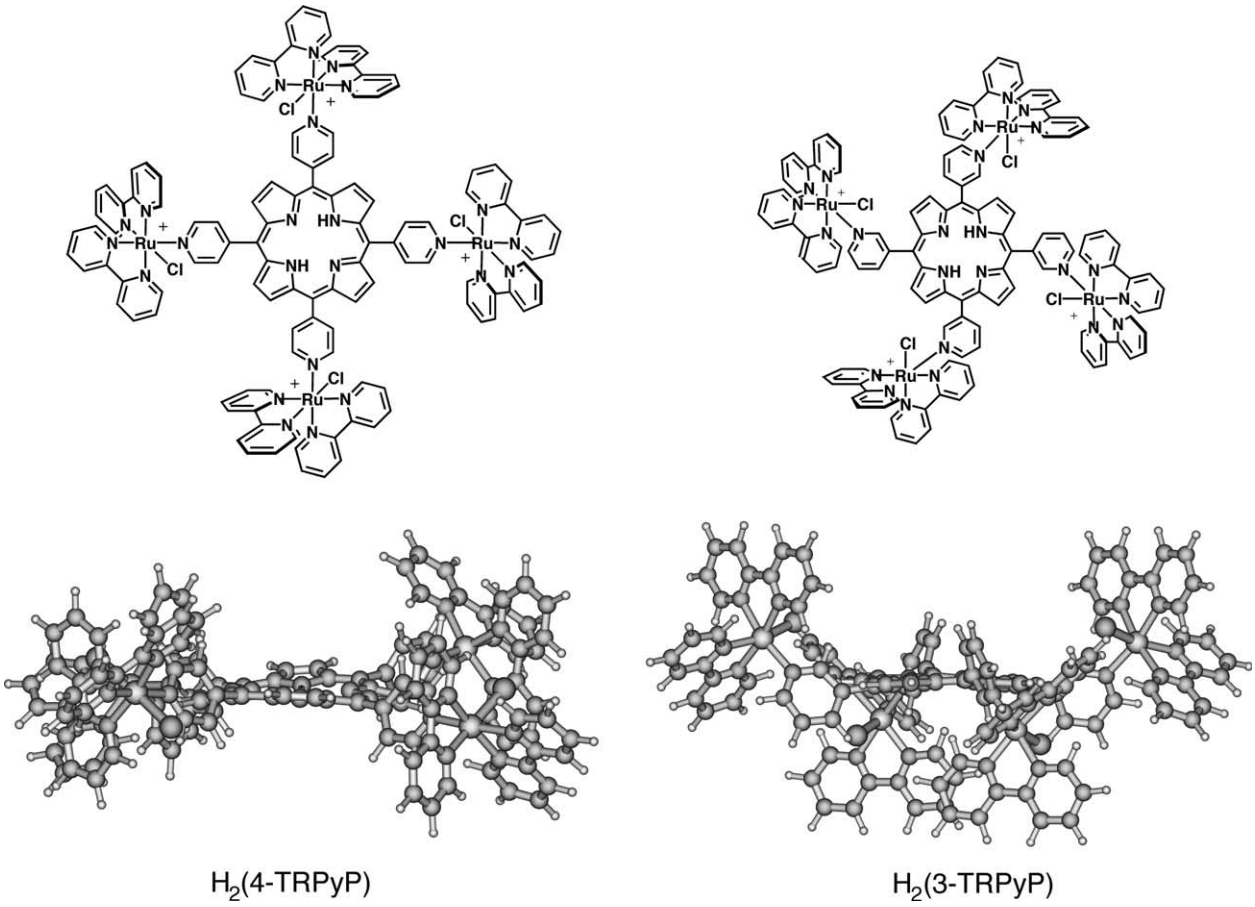

Fig. 1. Schematic and respective lateral view of the geometry optimized structures of the H_2(4-TRPyP) and H_2(3-TRPyP) complexes.

porphyrin chemistry with the ruthenium complex chemistry, generating interesting catalytic, electrocatalytic and photochemically active materials [30,32–35]. A remarkable aspect is that the $[Ru(bpy)_2Cl]^+$ derivatives can easily form quite homogeneous, electrochemically active and conducting molecular films, which may be useful for the preparation of amperometric detectors [36–38] based on modified electrodes. In addition, those porphyrins can form nanomaterials exhibiting enhanced electrocatalytic properties, by electrostatic assembly [19,39]. In order to provide a better understanding on the electronic structure and properties of those materials, the tetraruthenated porphyrins shown in Fig. 1 were investigated, by following a comparative approach, using molecular modeling calculations as support for the interpretation of the electrochemistry and spectroscopic data.

2. Experimental

5,10,15,20-Tetra(3-pyridyl)porphyrin, H_2(3-TPyP), was synthesized by the condensation of pyrrol (0.145 mmol) and 3-pyridylcarboxaldehyde (0.145 mmol), in refluxing acetic acid for an hour [40]. The viscous black tar obtained after solvent removal was treated with a dimethylformamide/ethanol 1:1 mixture and filtered. The bright violet solid was purified by silica gel column chromatography, using dichloromethane/ethanol 95:5 mixture as eluent. Yield: 20%. *Anal.* Calc. for $C_{40}H_{26}N_8$ (H_2(3-TPyP), 618.70 g mol^{-1}): C, 77.60; H, 4.21; N, 18.10. Found: C, 76.40; H, 4.69; N, 17.98%. ^{1}H NMR (300 MHz, $CDCl_3$, TMS): $\delta = -2.80$ ppm(s; 2H; pyrrole NH); 7.77 ppm(dd; 4H); 8.53 ppm(d; 4H); 8.87 ppm(s; 8H); 9.07 ppm (dd; 4H); 9.46 ppm(s; 4H). 5,10,15,20-tetra(4-pyridyl)porphyrin, H_2(4-TPyP), was purchased from Aldrich and used without further purification.

5,10,15,20-Tetra(3-methylpyridinium)porphyrin, $[H_2(3\text{-TMPyP})]Cl_4 \cdot 6H_2O$, and 5,10,15,20-tetra(4-methylpyridinium)porphyrin, $[H_2(4\text{-TMPyP})]Cl_4 \cdot 9H_2O$, were obtained by refluxing the corresponding *meso*-tetrapyridylporphyrins with an excess of methyltosylate in *N*,*N*-dimethylformamide (DMF) for 4 h (95% yield), according to the method described by Pasternack et al. [41]. *Anal.* Calc. for $C_{44}H_{38}N_8Cl_4 \cdot 6H_2O$ (H_2(3-TMPyP), 928.74 g mol^{-1}): C, 56.90; H, 5.43; N, 12.07. Found: C, 56.03; H, 5.78; N, 12.02%. ^{1}H NMR (300 MHz, acetone-d_6, TMS): $\delta = 10.07$ ppm(s, 4H); 9.61

ppm(d, 4H, $J_1 = 0.02$ ppm); 9.49 ppm(d, 4H, $J_1 = 0.02$ ppm); 9.24 ppm(s, 8H), 8.73 ppm(t, 4H, $J_1 = 0.02$ ppm), 4.93 ppm(s, 12H) and −2.99 ppm(s, 2H). *Anal.* Calc. for $C_{44}H_{38}N_8Cl_4 \cdot 9H_2O$ (H_2(4-TMPyP), 982.79 mg mol^{-1}): C, 53.77; H, 5.74; N, 11.40. Found: C, 53.60; H, 5.64; N, 11.27%. ^{1}H NMR (300 MHz, DMSO-d_6, TMS): $\delta = 9.47$ ppm(d, 8H, $J_1 = 0.02$ ppm); 9.81 ppm(s, 8H); 8.98(d, 8H, $J_1 = 0.02$ ppm); 4.72 ppm(s, 12H) and −3.10 ppm(s, 2H).

Octakis(2,2′-bipyridyl-1κ^2N,1κ$^2N'$,2κ^2N,2κ$^2N'$,3κ^2N,-3κ$^2N'$,4κ^2N,4κ$^2N'$)tetrachloro-1κCl,2κCl,3κCl,4κCl-(μ$_4$-5,10,15,20-tetra(3-pyridyl-1κN:2κN':3κN'':4κN'''-porphyrin)) tetraruthenium-(4+)tetrakis(trifluoromethanesulfonate), [H_2(3-TRPyP)](TFMS)$_4$, was obtained by the reaction of 200 mg of H_2(3-TPyP) with 630 mg of [Ru(bpy)$_2$Cl$_2$] (1:4.1 molar ratio), in refluxing glacial acetic acid for an hour, as described previously [31]. The final purification was carried out by neutral alumina column chromatography, using a mixture of dichloromethane/ethanol 9:1 as eluent. Yield: 95%. *Anal.* Calc. for $C_{120}H_{90}N_{24}Ru_4Cl_4(CF_3SO_3)_4 \cdot 12H_2O$ (3226.7 g/mol): C, 46.15; H, 3.56; N, 10.42. Found: C, 46.02; H, 3.49; N, 10.22%. ^{1}H NMR (300 MHz, acetone-d_6, TMS): −3.28 ppm (s, 2, NH); 7 to 10 ppm range (broad envelope, 88H). The number of water molecules was determined by thermogravimetry using the same sample sent for elemental analysis. The synthesis and characterization of [H_2(4-TRPyP)] and *cis*-dichloro-bis(2,2′-bipyridine)ruthenium(II) complex, [Ru(bpy)$_2$Cl$_2$], were previously described [31].

Molecular modeling calculations were carried out for H_2(3-TRPyP), H_2(4-TRPyP) and the respective protonated species, starting with the MM+ and a modified MM2(91) force field [42] for geometry optimization, employing the HYPERCHEM™ program [43]. A gradient of 10^{-3} kcal mol^{-1} Å^{-1} was used as convergence criterion in a conjugated gradient method. SCF molecular orbital calculations were performed at the RHF level, using the ZINDO/S method [44–47] and the default parameters (scaling factors $\kappa_{p\sigma} = 1.267$ and $\kappa_{p\pi} = 0.585$) or the PM3(tm) method [48] and a 10^{-7} kcal mol^{-1} as convergence criterion. Geometry optimization was successively refined using the atomic charge distribution, resulting from the semi-empirical calculations, until reaching convergence. The electronic spectrum was calculated based on single CI excitations using an active space of 25 frontier molecular orbitals (15 highest occupied and 10 lowest unoccupied MOs). For the model compounds, geometry optimizations were carried out using a gradient of 10^{-3} kcal mol^{-1} Å^{-1} in a conjugated gradient method. In these cases, DFT ab initio RHF/SCF molecular orbitals were obtained after the density matrix reached 10^{-7} kcal mol^{-1} of convergence.

The cyclic voltammograms were obtained in CH_3CN and DMF, using an AUTOLAB PGSTAT30 Potentiostat/Galvanostat. A conventional three electrodes cell was employed, consisting of a platinum disk working electrode, Ag/Ag^+ (0.010 M, in acetonitrile) reference electrode and a coiled platinum wire auxiliary electrode. The UV–Vis spectra were recorded on a HP-8453A diode-array spectrophotometer, in the 190 to 1100 nm range. The luminescence spectra were recorded on a Photon Technology Inc., model LS-100 spectrofluorimeter. The luminescence quantum yields were determined utilizing H_2(4-TMPyP) in water as standard ($\phi_{std} = 0.047$) [40,49,50] and the relationship $\phi = \phi_{std}(Abs_{std}/Abs)(Int/Int_{std})$, where Abs_{std} and Abs, and Int_{std} and Int are the absorbance at the excitation wavelength and the integrated fluorescence of the standard and the sample, respectively. The triplet state lifetimes were measured on a flash-photolysis equipment (Edinburgh Analytical Instruments) using a pulsed Nd:YAG laser (Spectron Laser System, England) operating at 355nm, for sample excitation. The analysis system, constituted by a 150 W pulsed xenon lamp, a Czern-Turner monochromator and a germanium detector for the near infrared, coupled with a Hewlett–Packard 54510B digital oscilloscope for data acquisition, was positioned at 90° ($\lambda = 420$ nm). The samples were purged for 15 min with 99.99% argon immediately before use.

Electrospray mass spectra were recorded on a Q-Tof mass spectrometer (Micromass) with a quadrupole (Qq) and high-resolution orthogonal time-of-flight configuration (*o*-TOF). The samples dissolved in methanol were injected with a syringe-pump (Harvard Apparatus, Pump 11, 10 μl/min) and the spectra acquired using an ESI capillary voltage of 3 kV and a cone voltage of 10 V. A sequential inductively coupled plasma optical spectrometer (Spectro Analytical Instruments GmbH, Kleve, Germany) equipped with a quartz spray chamber torch and concentric nebulizer (Meihard, TR-20-C1) was used for ruthenium determination by atomic fluorescence at $\lambda = 349.9$ nm. The atomic absorption spectra were collected in a SIMAA-6000 electrothermal spectrometer; which was equipped with a longitudinal Zeeman effect background correction system, Echelle optical arrangement solid-state detector and standard THGA graphite tube (Perkin–Elmer, Norwalk, CT, USA), in single-element mode (ruthenium cathode, $\lambda = 349.9$ nm, $i = 300$ mA), and calibrated with [Ru(bpy)$_3$]Cl$_2$.

3. Results and discussion

All compounds exhibited well resolved characteristic ^{1}H NMR peaks, except for H_2(3-TRPyP), in which the signals of the 2,2′-bipyridine ligand and the H_2(3-TPyP) β-pyrrolic and pyridyl protons in the 7 to 10 ppm range were superimposed, giving an integrated signal corresponding to 88H, consistent with the expected structure.

The singlet at −3.28 ppm (2H) was assigned to the inner ring protons. The mass spectrometry at low cone potential (~10 V) exhibited a set of major signals centered at $m/z = 604$ corresponding to the $[C_{120}H_{90}N_{24}Cl_4Ru_4]^{4+}$ molecular ion [51], which matched perfectly with the simulated spectrum.

The structures of the supramolecular porphyrins were further confirmed by determining the average number of coordinated $[Ru(bipy)_2Cl]^+$ complexes in H_2(TRPyP) supermolecules by measuring the ruthenium content at 2200 °C, by atomic absorption and emission techniques. In the first one, the pyrolysis and atomization processes were carried out at 1300 and 2200 °C, respectively, after a judicious study aiming the optimization of the analysis procedure. The pyrolysis temperature was carefully chosen for complete removal of the organic matrix that may interfere in the atomization process, without loosing ruthenium from the sample. An average content of 68.2 (±0.8) μg dm^{-3} of ruthenium was determined for a 68.60 μg dm^{-3} aqueous solution of H_2(3-TRPyP), as expected for a supermolecule with four $[Ru(bipy)_2Cl]^+$ complexes bound to the pyridylporphyrin N-atoms. This result was confirmed by atomic emission spectroscopy which gave a ruthenium content of 0.100 mg dm^{-3} (0.990 μM) for a 0.800 mg dm^{-3} aqueous solution of H_2(3-TRPyP) (0.992 μM in ruthenium).

3.1. Molecular modeling

Molecular modeling calculations were carried out for the tetraruthenated porphyrin species using molecular mechanics and ZINDO/S methods. In order to obtain a properly optimized geometry for such a multicomponent supramolecular species, current methods based on more rigorous quantum mechanics calculations are difficult to use, mainly because of the still too long computational time necessary in methods such as DFT. Molecular mechanics approach is much faster, however, it seems not to be adequate because of the supposedly higher deviations involved. However, Norrby and coworkers [52] have already developed rather suitable parameters for ruthenium polypyridyl complexes in which the Ru(II) ion is coordinated to six N-atoms like in the $[Ru(bpy)_3]^{2+}$ complex, based on a simplex method. For this reason, we started performing an extensive work on geometry optimization based on MM2(91) force field, pursuing the determination of good parameters for other ruthenium polypyridine complexes by using the available X-ray structural data as comparative references. In this way, we successfully extended Norrby's parameterization to complexes such as $[Ru(bpy)_2Cl(X)]$ and $[Ru(tpy)(bpz)Cl]^+$ [53–55], where X = Cl^- and 4,4′-bpy and bpz = 2,2′-bipyrazine, respectively, based on Allinger, Badger and Halgren's strategy [56–59]. Such parameters, e.g., Ru–Cl bonds stretching constant = 1.55 md $Å^{-2}$ (considering an equilibrium distance of 2.42 Å) and N–Ru–Cl bending parameter = 0.56 md Å rad^{-2} (for an equilibrium angle of 91.5°), were critically tested for geometry optimization by comparison with the XRD crystallographic structures and DFT calculations (Fig. 2). Those complexes were chosen because of the structural similarity with the peripheral groups of H_2TRPyP supramolecular porphyrins. The calculations were carried out using three levels of theory: the new force field, semi-empirical PM3(tm) and ab initio DFT. The results are quite good and some selected calculated bond distances are compared with that obtained by XRD in Table 1. It is possible to note that the new force field is sometimes better than ab initio calculations. The mean errors of the structures obtained by MM2(91), PM3(tm) and DFT methods are −2.3%, −3.4%, and 3.1%, respectively, relative to the XRD data. Excellent matching was obtained for the H_4TPP^{2+} porphyrin ring (Fig. 2, Table 2) [60], where TPP = 5,10,15,20-tetraphenylporphyrin, conveying enough confidence for the use of our strategy for the structural optimization of molecular systems constituted by quite a large number of atoms like the supramolecular porphyrins. Unfortunately, the XRD structures are influenced by molecular interactions that are neglected in the calculations in the vacuum and significant differences can appear, for example, in the phenyl ring dihedral angles, which are strongly influenced by π-stacking in the crystal. In fact, the calculated structure showed a 30° dihedral angle, while in the XRD structure it is equal to 60°.

Although the optimized structures of both supramolecular porphyrins display C_2 global symmetry, it should be noted that in the case of H_2(4-TRPyP) species the ruthenium ions are in the porphyrin ring plane, while in the H_2(3-TRPyP) isomer two $[Ru(bpy)_2Cl]^+$ groups at opposite corners are above and the other two are below the porphyrin ring, as shown in Fig. 1. As one can see by inspection of Tables 1 and 2, the geometries of the peripheral ruthenium complexes in the supermolecular porphyrins are in good agreement with those reported for related ruthenium polypyridyl complexes and porphyrin crystallographic data.

The electronic coupling of the ruthenium complexes and the porphyrin ring is dependent on the pyridyl bridge dihedral angle and can be insignificant when it becomes orthogonal to the macrocyclic ring. In fact, dihedral angles of 50–60° were found for the supramolecular species H_2(3-TRPyP) (50–53°); H_2(4-TRPyP) (57–59°); H_4(3-TRPyP) (48–56°) and H_4(4-TRPyP) (55–58°). In general, that angle was lower for the *meta*- in comparison with the *para*-isomer, as expected for a lower steric hindrance between the *ortho*-pyridyl and β-pyrrole H-atoms caused by a saddle distortion of the porphyrin ring. This was consistently higher in the optimized structure of the *meta*-isomer and was enhanced by

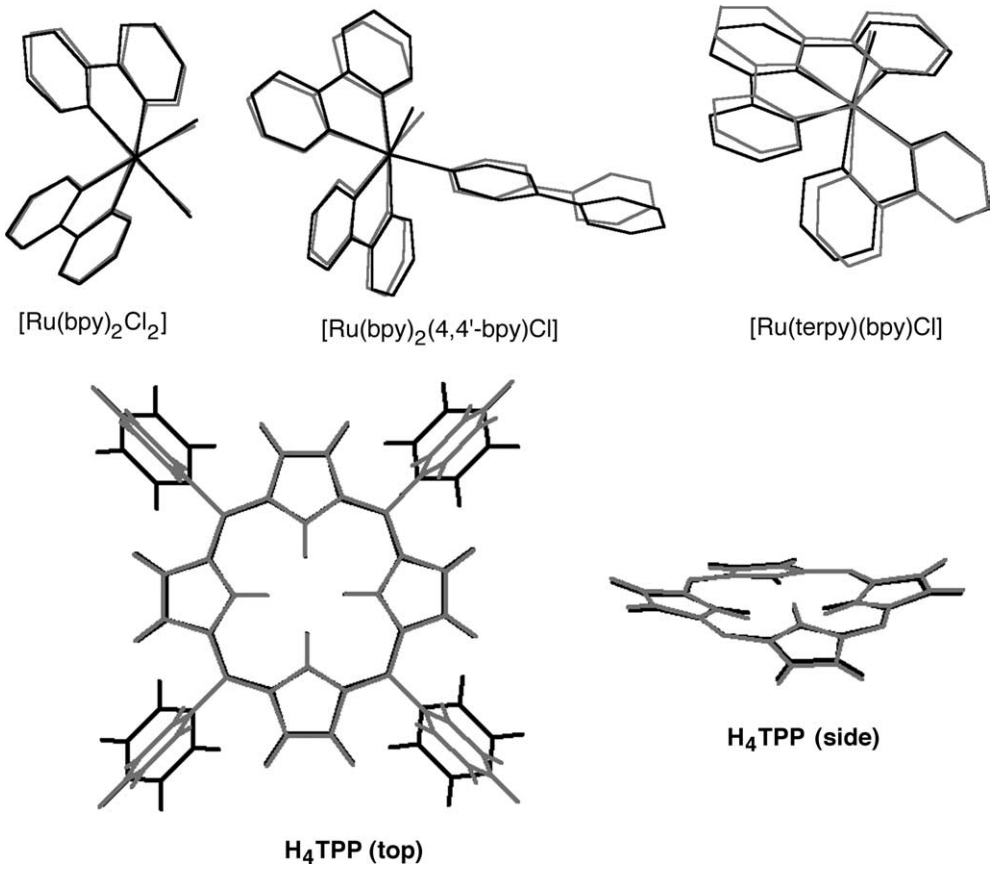

Fig. 2. Structures of $[Ru(bpy)_2Cl_2]$, $[Ru(bpy)_2(4,4'\text{-bpy})Cl]^+$ and $[Ru(tpy)(bpy)Cl]^+$ complexes, and top and side (the phenyl rings were omitted) views of H_4TPP^{2+} optimized by MM2(91) method in comparison with the X-ray diffraction structure (gray).

the bis-protonation because of the intense electrostatic repulsion between the inner acidic hydrogen atoms.

The relevant HOMO and LUMO levels obtained by SCF calculations and the fractional mixture of the frontier orbitals are listed in Tables 3 and 4.

The HOMO (MO 373) of H_2(4-TRPyP) species has a_{2u} symmetry and is predominantly localized on the ruthenium polypyridyl complexes (66%), but possesses a substantial contribution from the porphyrin moiety (24%), where the electronic density is concentrated on the pyrrole nitrogen and *meso*-carbon atoms (Table 3). The two lowest energy LUMOs (MO 374 and 375) are highly localized on the porphyrin ring. The bridging pyridyl groups contribute with about 10% for the HOMO and LUMO composition, favoring the electronic coupling of the porphyrin with the peripheral ruthenium complexes in the ground and excited states. In addition, the relative conformations of these

Table 1
Selected X-ray diffraction and calculated (by MM2(91), PM3(tm) and DFT methods) bond lengths and respective errors (%)

Bonds	XRD	MM2(91)	PM3(tm)	DFT
$[Ru(bpy)_2Cl_2]$				
Ru–Cl[a]	2.426	2.449 (0.95%)	2.376 (−2.1%)	2.499 (3.0%)
Ru–N(bpy)[a]	2.034	2.112 (3.8%)	2.014 (−0.82%)	2.057 (1.1%)
$[Ru(bpy)_2(4,4'\text{-bpy})Cl]^+$				
Ru–Cl	2.433	2.446 (0.53%)	2.402 (−1.3%)	2.501 (2.8%)
Ru–N(bpy)[a]	2.051	2.111 (2.9%)	2.038 (−0.53%)	2.076 (1.2%)
Ru–N(44′bpy)	2.116	2.124 (0.38%)	2.064 (−2.1%)	2.158 (2.0%)
$[Ru(tpy)_2(bpz)Cl]^+$				
Ru–Cl	2.405	2.432 (1.1%)	2.366 (−1.6%)	2.463 (2.4%)
Ru–N(bpz)[a]	2.035	2.102 (3.3%)	2.022 (−0.53%)	2.071 (1.8%)
Ru–N(tpy)[a]	2.073	2.103 (1.4%)	2.045 (−1.2%)	2.098 (1.2%)

[a] Average values.

Table 2
Selected bond lengths of H_2TRPyP supramolecular porphyrins and H_4TPP^{2+} calculated by MM2(91) method and from X-ray diffraction

Bond	H_4TPP^{2+} (XRD)	H_4TPP^{2+} (MM2)	H_2(3-TRPyP)	H_2(4-TRPyP)
Ru–Cl			2.458	2.445
Ru–N(bpy)*			2.115	2.118
Ru–N(pyP)			2.128	2.132
C1–C2	1.442	1.400	1.398	1.399
C2–C3	1.348	1.389	1.386	1.386
C4–C5	1.399	1.404	1.401	1.401
C1–N21	1.384	1.276	1.276	1.276
N21–H	1.018	1.041	1.048	1.048

* Nitrogen atom *trans* to the bridging pyridyl group.

complexes can change without increasing very much the energy because of the relatively low steric hindrance.

In contrast, the HOMO (MO 373) of the *meta*-isomer comes out to be essentially localized (89%) at the peripheral ruthenium complexes (Fig. 3 and Table 4), including the pyridyl bridging groups (9%), while the contribution of the porphyrin ring is very small (<2%). On the other hand, the two lowest energy LUMOs (MO 374 and 375) are essentially localized on the porphyrin ring (91%) and on the pyridyl-bridging group (9%), in analogy with the *para*-isomer. This means that the excited state properties will be controlled by the porphyrin moiety in both cases, but significant differences are expected as a consequence of the orbital mixture observed specially for the H_2(4-TRPyP) species.

DFT calculations have been used to explain the strong coupling observed between the porphyrin ring and the *meso*-phenyl substituents in TPP [29,61]. Similar effects are expected for the *meso*-pyridylporphyrins. Accordingly, the calculations are reflecting the much stronger electronic coupling between the peripheral ruthenium bipyridyl complexes and the porphyrin ring in the H_2(4-TRPyP) isomer. This result probably is reflecting the presence of a nodal plane at the pyridyl-bridge of H_2(3-TRPyP), whereas in the(4-TRPyP) isomer such node is absent. On the other hand, the coupling should also be dependent on the dihedral angle between the porphyrin and bridging pyridyl rings, tending to disappear when they are orthogonal and reaching a maximum when both are coplanar. Our modeling results

Table 3
Selected H_2(4-TRPyP) HOMO and LUMO energy levels and respective molecular orbital composition (%) determined by SCF calculation (RHF-CI) using ZINDO/S method

MO	Energy (eV)	Ru	Cl	Pyridyl	Porphyrin	Bpy
384	−6.34	6.06	0.23	1.06	6.86	85.79
383	−6.38	4.43	0.28	7.00	1.23	87.05
382	−6.39	4.21	0.27	9.66	1.26	84.60
381	−6.39	4.18	0.27	10.59	0.73	84.23
380	−6.58	5.73	0.15	20.71	31.21	42.20
379	−6.75	4.81	0.09	5.98	1.80	87.31
378	−6.76	4.41	0.08	8.02	1.37	86.12
377	−6.77	4.25	0.08	8.96	0.58	86.13
376	−6.84	1.49	0.03	25.88	14.27	58.33
375	−7.94	0.43	0.01	6.93	92.07	0.57
LUMO 374	*−7.95*	*0.66*	*0.01*	*10.99*	*87.32*	*1.02*
HOMO 373	*−12.25*	*46.54*	*1.61*	*10.32*	*23.59*	*17.94*
372	−12.40	62.77	3.27	8.43	0.83	24.70
371	−12.40	62.80	3.28	8.34	0.88	24.71
370	−12.41	62.92	3.37	8.15	0.86	24.70
369	−12.61	71.49	3.74	3.13	7.40	14.24
368	−12.65	78.44	2.71	3.83	0.57	14.45
367	−12.65	78.72	2.72	3.80	0.25	14.50
366	−12.66	78.67	2.67	3.86	0.26	14.54
365	−12.74	74.47	4.75	0.78	3.17	16.84
364	−12.75	77.59	4.13	1.32	0.16	16.80
363	−12.75	77.65	4.12	1.34	0.08	16.81
362	−12.75	77.66	4.07	1.40	0.09	16.78
361	−12.92	27.60	0.10	9.90	54.75	7.64
360	−13.07	0.66	0.01	1.94	97.21	0.18
359	−14.19	0.54	0.21	0.11	0.01	99.14
358	−14.19	0.54	0.21	0.11	0.01	99.14
357	−14.19	0.54	0.21	0.11	0.01	99.14

Table 4
Selected H_2(3-TRPyP) HOMO and LUMO energy levels and respective molecular orbital composition (%) determined by SCF calculation (RHF-CI) using ZINDO/S method

MO	Energy (eV)	Ru	Cl	Pyridyl	Porphyrin	Bpy
384	−6.90	4.58	0.22	33.97	0.67	60.56
383	−6.91	4.60	0.21	38.15	0.79	56.24
382	−6.96	3.59	0.28	27.40	1.74	66.98
381	−6.96	3.59	0.28	25.64	0.67	69.82
380	−7.26	0.79	0.04	23.12	69.32	6.73
379	−7.36	5.37	0.14	7.31	0.24	86.93
378	−7.36	5.17	0.13	8.64	1.32	84.73
377	−7.42	3.75	0.07	13.00	0.35	82.83
376	−7.42	3.37	0.06	15.26	1.94	79.36
375	−8.66	0.09	0.01	8.68	91.09	0.13
LUMO 374	*−8.70*	*0.13*	*0.00*	*9.21*	*90.56*	*0.09*
HOMO 373	*−12.96*	*60.78*	*3.62*	*9.16*	*1.83*	*24.62*
372	−12.97	62.20	3.87	8.53	0.23	25.17
371	−13.00	61.47	3.84	6.40	4.94	23.36
370	−13.02	65.53	4.25	4.98	0.22	25.02
369	−13.17	75.84	3.10	5.66	0.75	14.64
368	−13.17	76.14	3.12	5.79	0.14	14.82
367	−13.23	54.61	1.75	8.45	24.39	10.80
366	−13.26	79.02	2.09	3.98	0.13	14.78
365	−13.29	60.76	3.54	5.03	17.98	12.69
364	−13.31	77.52	4.41	1.04	0.04	17.00
363	−13.32	73.51	3.73	2.64	3.76	16.36
362	−13.33	76.70	3.89	2.65	0.11	16.66
361	−13.37	48.80	2.06	6.83	31.53	10.77
360	−13.89	1.74	0.04	2.04	95.52	0.66
359	−14.69	0.56	0.28	0.06	0.02	99.09
358	−14.69	0.55	0.28	0.04	0.02	99.11
357	−14.71	0.64	0.23	0.14	0.02	98.97

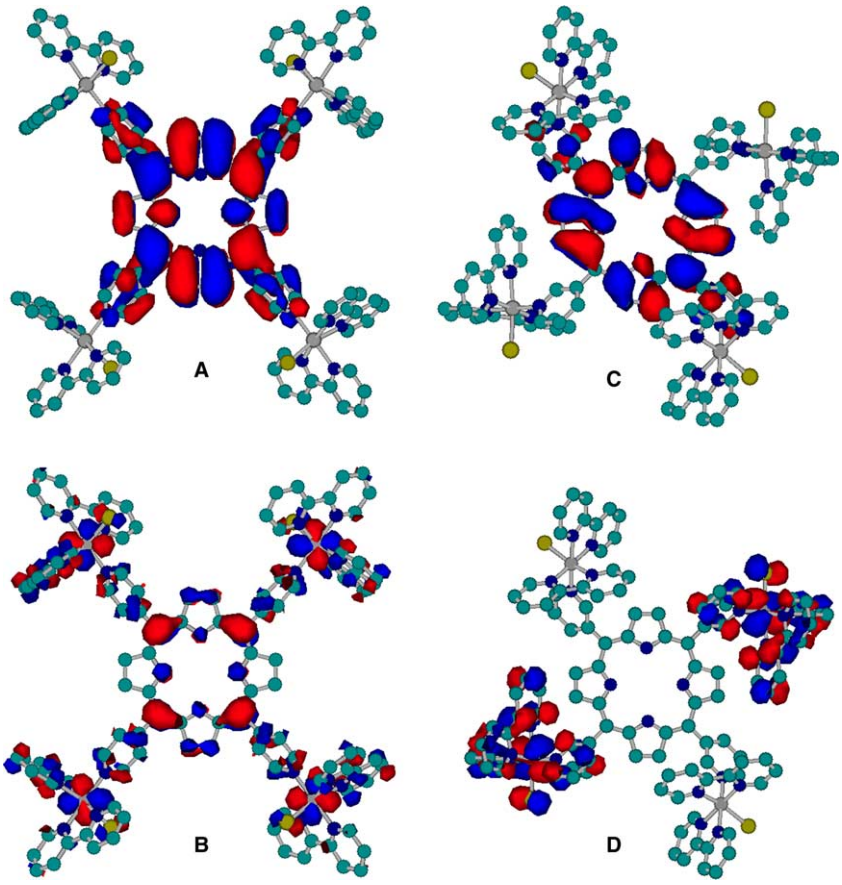

Fig. 3. (A,C) LUMO and (B,D) HOMO of H_2(4-TRPyP) (left) and H_2(3-TRPyP) (right). Hydrogen atoms were omitted for clarity.

showed that the dihedral angle is comparable in both isomers, indicating that the nodal plane at the pyridyl-bridge is playing a major role in controlling the electronic coupling between the central and peripheral groups.

3.2. Electronic spectra

The UV–Vis spectra of the H_2(3-TRPyP) and H_2(4-TRPyP) species in methanol (Fig. 5) exhibited the porphyrin Soret, $Q_{y(1-0)}$, $Q_{y(0-0)}$, $Q_{x(1-0)}$ and $Q_{x(0-0)}$ bands at 417 ($\log(\varepsilon) = 5.37$), 513 (4.56), 547 (4.13), 588 (3.96) and 650 (3.46), and 416 (5.33), 513 (4.66), 554 (4.37), 590 (4.13) and 648 (3.75), respectively. The parent H_2(3-TPyP) and H_2(4-TPyP) species exhibited the Soret, $Q_{y(1-0)}$, $Q_{y(0-0)}$, $Q_{x(1-0)}$ and $Q_{x(0-0)}$ bands at 413, 512, 545, 587 and 646 nm, respectively, in chloroform, showing a small perturbation of pyridylporphyrin spectra after the coordination of four $[Ru(bpy)_2Cl]^+$ groups. However, they added three new absorption bands to the characteristic spectra of porphyrins at 294, 360 and 480 nm, assigned to the 2,2′-bipyridine intraligand $p\pi-p\pi^*$ and two $Ru^{II}(d\pi) \rightarrow bpy(p\pi^*)$ charge-transfer transitions, respectively.

ZINDO/S CI calculations have been carried out for the parent H_2(3-TPyP) and H_2(4-TPyP) species and the corresponding tetraruthenated complexes. In the case of the porphyrin species, the ZINDO/S results matched the transition energies of the measured spectra and intense bands were predicted in the 400 nm (Soret) and weaker ones in the 500 to 700 nm range (Q bands). In the case of the supramolecular complexes, the large number of atoms and especially the presence of the ruthenium atoms introduced a high burden to the calculations. However, even in this more demanding case, the position of the $Ru(d\pi) \rightarrow bpy(p\pi^*)$ charge-transfer bands was reasonably predicted (393 and 483 nm for H_2(3-TRPyP), and 388 and 509 nm for H_2(4-TRPyP), respectively, for the MLCT1 and MLCT2 transitions, Tables 5 and 6) by the ZINDO/S method. Strong contributions of $Ru^{II}(d\pi) \rightarrow pyP(p\pi^*)$ charge-transfer transitions were also predicted in the 400 to 510 nm region for both species. Because of the strong spectral superimposition, no evidence of such bands has been found in the UV–Vis spectra of both isomers but is showing up as band broadening, particularly in the case of H_2(4-TRPyP) species, as expected for a higher electronic coupling and orbital mixing. However, the $Ru^{II}(d\pi) \rightarrow pyP(p\pi^*)$ charge-transfer transition has been observed

Table 5
Electronic spectrum of H_2(3-TRPyP) in methanol (λ_{exp}) and calculated electronic transitions by ZINDO/S CI (λ_{calc}) and orbitals contributing in the ground (MO_i) and excited (MO_f) states of the supermolecular species, respectively

λ_{exp} (nm)	λ_{calc} (nm)	Calculated intensity	$MO_i \rightarrow MO_f$	Assignment
H_2(3-TRPyP)				
650 (Q_{0-0})	680	w	360, 361, 367 → 374, 375	Q bands
588 (Q_{0-1})				
547 (Q_{0-0})	612	m	360 → 374, 375	
513 (Q_{0-1})				
[a]	505	m	368, 371, 373 → 374, 375 ($Ru^{II}(d\pi) \rightarrow pyP(p\pi^*)$)	MLCT bands
~480[a]	483	m	368, 370, 371 → 378, 379, 374 ($Ru^{II}(d\pi) \rightarrow bpy(p\pi^*)$)	
[a]	445	m	363 → 375 ($Ru^{II}(d\pi) \rightarrow pyP(p\pi^*)$)	
360	393	w	363, 364 → 381, 382 ($Ru^{II}(d\pi) \rightarrow bpy(p\pi^*)$)	
417	351	s	360 → 374, 375	Soret band

w = weak (<0.1); m = medium (0.1–1), s = strong (>0.5).
[a] Broad band envelope.

Table 6
Electronic spectrum of H_2(4-TRPyP) in methanol and selected calculated electronic transitions by ZINDO/S CI and orbitals contributing in the ground (MO_i) and excited (MO_f) states of the supermolecular species, respectively

λ_{exp} (nm)[a]	λ_{calc} (nm)	Calculated intensity	$MO_i \rightarrow MO_f$	Assignment
H_2(4-TRPyP)				
648 (Q_{0-0})	676	w	360, 361, 373 → 374, 375	Q bands
590 (Q_{0-1})				
554 (Q_{0-0})	616	m	360, 373 → 374, 375	
513 (Q_{0-1})				
~480[a]	501	s	363, 364 → 377, 379 ($Ru^{II}(d\pi) \rightarrow bpy(p\pi^*)$)	MLCT bands
[a]	442	m	372, 373 → 374, 375 ($Ru^{II}(d\pi) \rightarrow pyP(p\pi^*)$)	
[a]	405	w	364, 365 → 374 ($Ru^{II}(d\pi) \rightarrow pyP(p\pi^*)$)	
365	389	m	($Ru^{II}(d\pi) \rightarrow bpy(p\pi^*)$)[b]	
416	347	s	360, 361 → 374, 375	Soret band

w = weak (<0.1); m = medium (0.1–1); s = strong (>0.5).
[a] Broad band envelope.
[b] Probable assignment.

for the Zn(4-TRPyP)/H_2TPPS ion-pair species at 460 nm, in methanol [62], showing a good matching with the calculated result (442 nm for H_2(4-TRPyP)).

3.3. Protonation effects in the electronic spectra

The H_2(3-TRPyP) and H_2(4-TRPyP) species can undergo bis-protonation at the porphyrin center, leading to significant spectral changes, as illustrated in Fig. 5. The H_2(3-TRPyP) isomer exhibited a spectrum [63] that resembles the sum of the ruthenium complex and the protonated-porphyrin absorption bands, showing the characteristic red-shifted Soret band at 444 nm and a couple of narrow Q bands at 600 ($\log(\varepsilon) = 4.05$) and 650 (4.39) nm, in methanol. The H_4(4-TRPyP) species exhibited drastic differences. In addition to the bpy intraligand $p\pi - p\pi^*$ at 294 nm and the Soret band at 443 nm, the typical porphyrin spectral profile with two sharp bands in the visible was replaced by two broad features at 560 (3.9) and 704 (4.52) nm, in acidified methanol solution. The energy difference between these bands (3650 cm^{-1}) is more than twice that normally found between the Q bands of H_4-TMPyP. Also, they are solvent sensitive and the lower energy band was shifted to 690 nm in aqueous HCl solution and 712 nm in CH_3CN. Its assignment to a $Ru^{II}(d\pi) \rightarrow H_4$-(4-TPyP)$^{2+}$ charge-transfer transition is consistent with the ZINDO/S CI modeling results and was confirmed by spectroelectrochemistry [64]. The porphyrin π orbitals are stabilized by the bis-protonation of the ring, consequently increasing the contribution of ruthenium orbitals in the HOMO (compare Figs. 3 and 4). In fact, for the H_4(4-TRPyP)$^{2+}$ species, a medium intensity band was predicted by the theoretical calculations at 1468 nm (6812 cm^{-1}), corresponding to the ruthenium-to-protonated porphyrin charge-transfer transition. The red-shift with respect to the predicted ruthenium-to-porphyrin MLCT band at 442 nm in the H_2(4-TRPyP) species is qualitatively consistent with the increased facility to reduce the protonated porphyrin ring. However, in comparison with the experimental band at 704 nm (14204.5 cm^{-1}) the energy matching is poor. More rea-

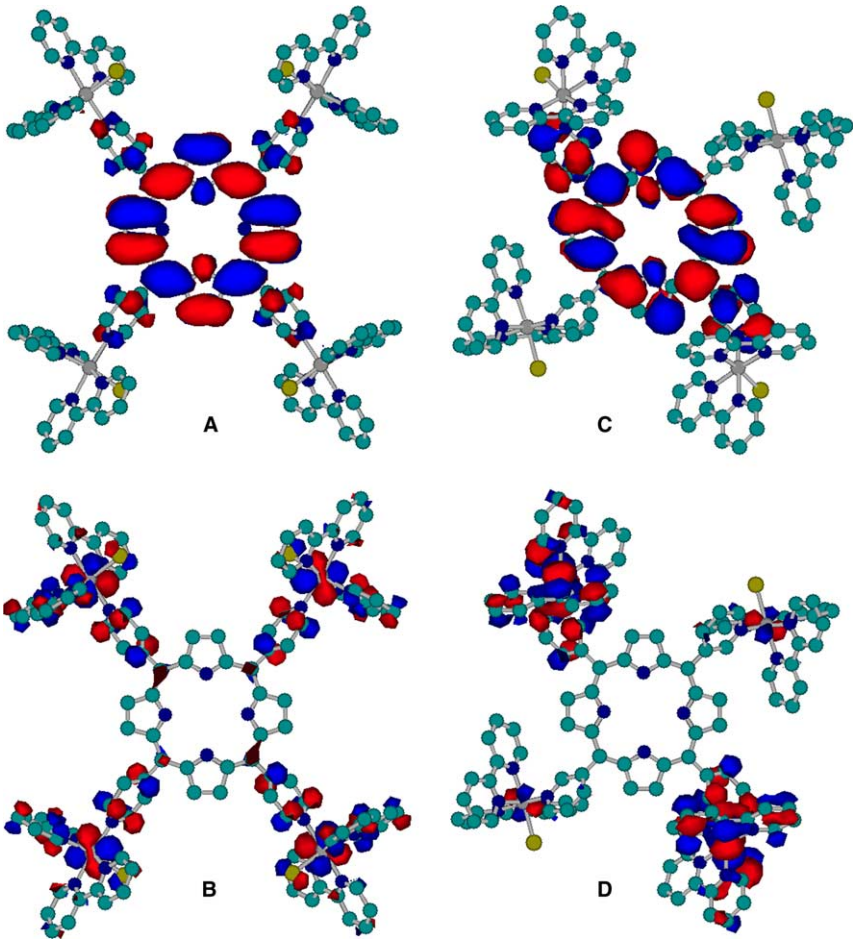

Fig. 4. LUMO (A) and HOMO (B) of H_4(4-TRPyP)$^{2+}$; LUMO (C) and HOMO (D) of H_4(3-TRPyP)$^{2+}$. Hydrogen atoms were omitted for clarity.

sonable agreement between the calculated and experimental transition energies was found for the porphyrin Q and Soret bands. In this case, a deviation of up to 20% was observed, indicating that the semi-empirical approximations should be improved further in order to obtain more rigorous quantitative predictions. A similar charge-transfer transition was predicted for the H_4(3-TRPyP)$^{2+}$ isomer as well but with much lower intensities. In fact, no band was observed experimentally. This is consistent with a smaller transition moment integral as consequence of a less effective electronic coupling between the peripheral ruthenium complexes and the porphyrin ring.

Furthermore, the comparison of TPP-like porphyrins with peripherally crowded nonplanar porphyrins such as octaethyltetraphenylporphyrin and dodecaphenylporphyrin suggested that the red-shift of the absorption bands can arise from ring distortions [61,65]. However, recently, Rosa et al. [29] showed by time-dependent DFT calculations that it is a consequence of the strong π-interactions between the porphyrin and the phenyl rings in H_4TPP^{2+}. Similar behavior is expected for pyridilporphyrins, as can be inferred from the spectral characteristics of H_4TPyP^{2+}, H_4TMPyP^{2+} and H_4TRPyP^{2+} species. Red-shifted and broadened Soret bands in comparison with the corresponding non-protonated species were observed in these cases also, reinforcing the possibility of a $Ru^{II}(d\pi) \rightarrow pyP(p\pi^*)$ charge-transfer transition in our supramolecular porphyrin system.

3.4. Luminescence spectra

The fluorescence spectra of H_2(4-TRPyP) and H_2(3-TRPyP) exhibited the $Q_{(0,1)}$ and $Q_{(0,0)}$ transitions at 652 and 703, and 654 and 708 nm, respectively, at room temperature, in analogy with H_2(4-TMPyP). This indicates that the lowest luminescent excited state is localized on the porphyrin ring, as predicted by the theoretical calculations. The emission energies were only slightly perturbed, but the coordination of four $[Ru(bpy)_2Cl]^+$ groups to the pyridylporphyrin N-atoms decreased the fluorescence quantum-yield by two and three orders of magnitude ($\phi_{fl} \sim 1 \times 10^{-4}$ and $\sim 2 \times 10^{-5}$) for the *para*- and *meta*-isomers, respectively. This should arise from the enhancement of thermal relaxation and intersystem-crossing efficiencies induced by

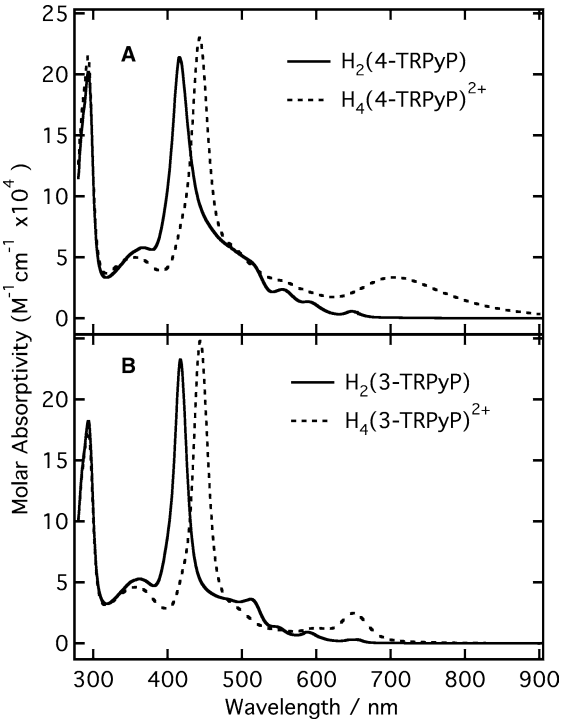

Fig. 5. UV–Vis spectra of ~3.0 μM solutions of protonated (dashed lines) and non-protonated (solid lines) (A) H_2(4-TRPyP) and (B) H_2(3-TRPyP), in methanol. The protonation was carried out by dissolving gaseous HCl into the solution.

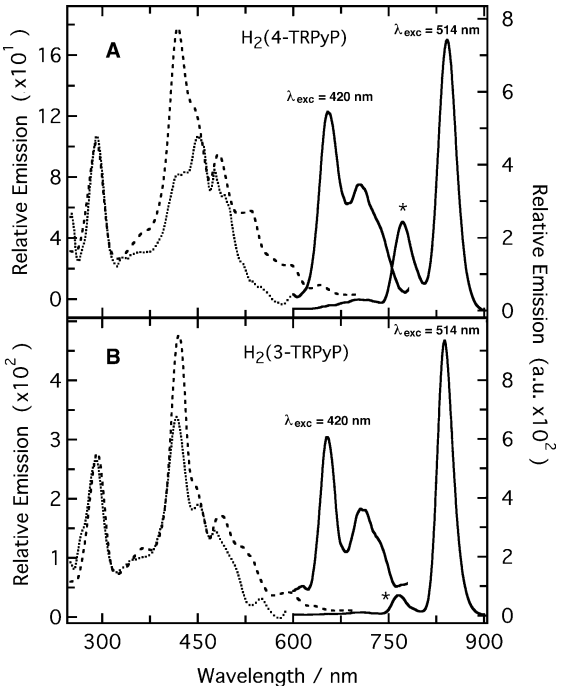

Fig. 6. Luminescent emission (right axis; λ_{exc} = 420 and 514 nm) and excitation spectra (left axis; λ_{em} = 655 (dashed line) and 840 nm (dotted line)) of (A) H_2(4-TRPyP) and (B) H_2(3-TRPyP) supermolecules, in ethanol glass, at 77 K. * scattering.

the peripherally bound ruthenium complexes, as well as the higher dipole moment (μ_{meta} = 10.3 D; μ_{para} = 0.0 D, by ZINDO/S method) predicted for the H_2(3-TRPyP) species [29,61]. This same effect can be observed for the H_2(3-TMPyP) and H_2(4-TMPyP) species also, for which the triplet-state lifetime in methanol solution was determined to be 17.6 μs for H_2(4-TMPyP) and only 1.6 μs for the H_2(3-TMPyP) species. In the case of the supramolecular porphyrins, that effect is shadowed by the heavy atom effect and tuned by the electronic coupling between the porphyrin ring and the ruthenium complexes. In fact, the triplet-state lifetimes of the H_2(3-TRPyP) and H_2(4-TRPyP) species were found to be 1.9 and 0.21 μs, respectively.

The fluorescence and phosphorescence spectra of these species in ethanol glass matrix (77 K) are shown in Fig. 6. H_2(3-TRPyP) exhibits emission bands at 654, 710 and 842 nm (λ_{exc} = 420 and 514 nm), while the H_2(4-TRPyP) isomer showed the same bands at 655, 704 and 841 nm, respectively. However, the band at 840 nm was observed with higher intensity when the solution was excited at 514 nm, i.e., where the contribution of the ruthenium complexes MLCT band is predominant. The lowest emission band energy of both species compares well with that reported [40] for the phosphorescence band of H_2(4-TMPyP) in ethanol glass (860 nm) and was assigned accordingly. The excitation spectra obtained by monitoring at the fluorescence and phosphorescence emission bands (λ_{em} = 655 and 840 nm, respectively) matched the absorption spectrum of H_2(3-TRPyP) even at the Ru^{II}(dπ)-to-bpy(pπ*) charge-transfer band around 480 nm. Similar result was obtained for the *para*-isomer, strongly suggesting the occurrence of energy-transfer from the ruthenium complexes to the porphyrin singlet and triplet excited states, in both supermolecular porphyrins [18,31].

3.5. Electrochemistry

The electrochemistry of H_2(3-TRPyP) was studied by cyclic voltammetry (Fig. 7) exhibiting six redox processes in the −1.8 to 1.8 V range, which were confirmed by spectroelectrochemistry (Figs. 3 and 4). The processes below −0.5 V, attributed to the reduction of the porphyrin and 2,2′-bipyridine ligands, are better seen in DMF solution. The wave above 1.3 V, corresponding to the oxidation of the porphyrin ring, was better visualized in CH_3CN solution (inset Fig. 2). The oxidation wave at 1.57 V showed a scan rate dependent behavior, characteristic of an EC process and was assigned to the oxidation of the porphyrin ring followed by a chemical reaction, probably involving the solvent. The reversible Ru(III/II) process was found at $E_{1/2}$ = 0.88 V, which is 40 and 20 mV more negative than for the H_2(4-TRPyP) isomer (0.92 V) [64] and $[Ru(bpy)_2pyCl]^+$ complex [66], respectively, in DMF (Table 7). However, there is an inversion in such order in acetonitrile solution, and both

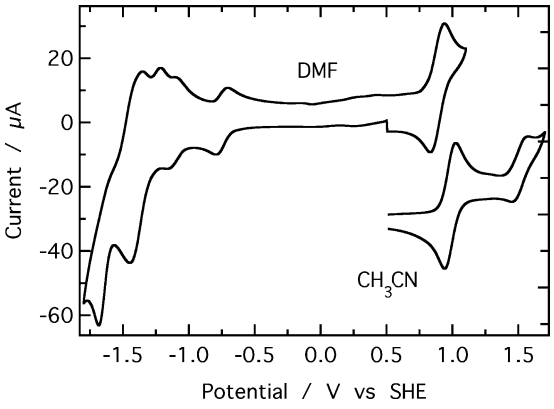

Fig. 7. Cyclic voltammogram of a 2.0×10^{-3} M solution of H_2(3-TRPyP) in DMF, 100 mV s^{-1}. Inset: Cyclic voltammogram of a 2.0×10^{-3} M solution in CH_3CN, in the 0.50 to 1.65 V range and DPV results for the Ru(III/II) and Porf(−1/0) process.

potentials become lower than that found for the $[Ru(bpy)_2pyCl]^+$ complex [67] (0.99 and 0.96 V, respectively, in comparison with 1.02 V). That anodic shift reflects the lower stabilization of the Ru(III) complex in the less polar solvent, and eventually can be used as a measure of the degree of charge localization in those complexes. As expected, the potential of the conventional pyridine complex was the most strongly shifted (120 mV), closely followed by H_2(3-TRPyP) (110 mV), while the potential of H_2(4-TRPyP) was shifted by only 40 mV. This suggests that the charge on the *meta*-substituted isomer is essentially localized as in the $[Ru(bpy)_2pyCl]$ complex. In contrast, extensive charge redistribution should be occurring in the *para*-isomer, as confirmed by the theoretical calculations. The HOMO and LUMO composition is also in accordance with the electrochemistry results, where the first oxidation occurred at the ruthenium complexes while the first reduction was porphyrin centered (Tables 3 and 4).

The two successive monoelectronic porphyrin ring reductions of *meta*- and *para*-H_2(TRPyP) to the radical anion and dianion were found at $E_{1/2} = -0.67$ and -1.06 V (Fig. 2) and at -0.68 and -0.93 V, respectively. This shows that the energy necessary to introduce the first electron is essentially the same, as expected for the virtually equivalent density of charge on the pyrrole N-atoms calculated by Mülliken population analysis ($q_{meta} = -0.480$; $q_{para} = -0.478$) for both isomers. There is a significant difference in the potential for the second

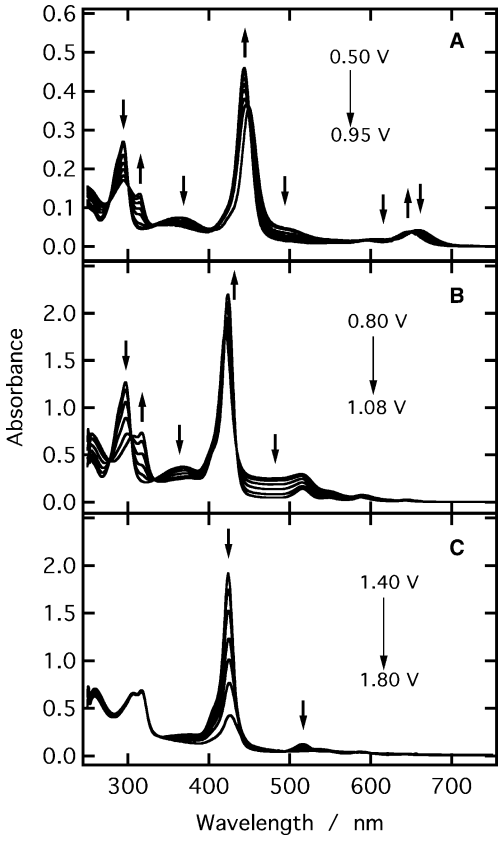

Fig. 8. Spectroelectrochemistry (A) of a 1×10^{-4} M H_4(3-TRPyP)$^{2+}$ in CH_3CN solution in the 0.50 to 0.95 V range; and of a 2.0×10^{-3} M H_2(3-TRPyP) in DMF solution in the (B) 0.80 to 1.08 V and (C) 1.40 to 1.80 V range. Electrolyte: 0.10 M $TEAClO_4$.

reduction (130 mV), however, which can be assigned to a higher electrostatic repulsion in the *meta*-isomer, because the extra electron is more efficiently delocalized into the peripheral groups in the *para*-species.

The reduction of the bipyridine ligands was not significantly influenced by the porphyrin moiety, such that the first monoelectronic process was found at $E_{pc} = -1.39$ V and the second at $E_{pc} = -1.63$ V for both species. The integrated charge under the Ru(III/II) and P(0/1–) waves of the cyclic voltammograms (Fig. 7) gave a 4:1 ratio for the ruthenium complexes to porphyrin moiety. This result was confirmed by differential pulse voltammetry. All redox potentials are listed in Table 7 including those of the H_2(4-TRPyP) species.

Table 7
Redox potentials (V vs. SHE) of H_2(TRPyP) in DMF solution

Compound	$Bpy^{-2/-1}$	$Bpy^{-1/0}$	$Porph^{-2/-1}$	$Porph^{-1/0}$	$Ru^{3+/2+}$	$Porph^{0/+1}$
H_2 (3-TRPyP)	−1.63	−1.39	−1.06	−0.67	0.88 (0.99)[a]	– (1.57)[a]
H_2 (4-TRPyP)		−1.42	−0.93	−0.68	0.92 (0.96)[a]	– (1.65)[a]

The potential of reversible processes was determined as the average of E_{pc} and E_{pa}, while E_{pc} (second reduction of the bpy ligands) and E_{pa} (oxidation of porphyrin ring) were listed for the irreversible processes.

[a] In CH_3CN solution.

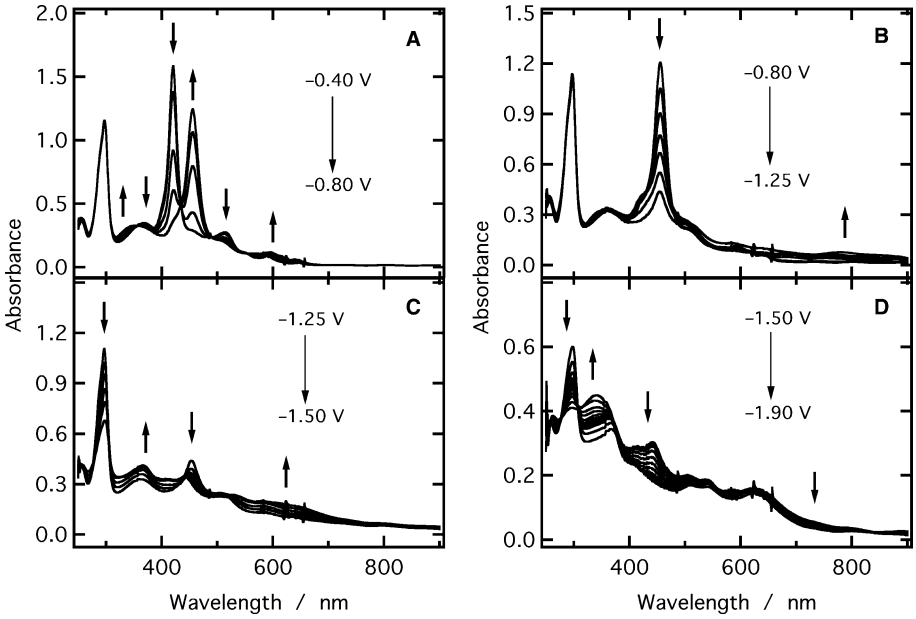

Fig. 9. Spectroelectrochemistry of 1.5×10^{-3} M H_2(3-TRPyP) in the (A) −0.40 to −0.80 V, (B) −0.80 to −1.25 V, (C) −1.25 to −1.50 V and (D) −1.50 to −1.90 V range. Electrolyte: 0.10 M $TEAClO_4$ in DMF.

The spectroelectrochemistry data were collected in DMF and CH_3CN. The oxidation of the H_2(3-TRPyP) supermolecule in the 0.80 to 1.08 V range (Fig. 8B, in CH_3CN) led to the disappearance of the $Ru^{II}(d\pi)$-to-bpy($p\pi^*$) charge-transfer band at 480 and 370 nm. Concomitantly, the bpy $p\pi \rightarrow p\pi^*$ band at 297 nm disappeared and two new bands rose at 299 and 317 nm, while the characteristic porphyrin absorption bands remained almost unchanged (the Soret band was 20% intensified and shifted 3 nm to the red). In fact, the spectrum of $[H_2(3\text{-TPyP})\{Ru^{III}(bpy)_2Cl\}_4]$ species above 350 nm is similar to that of H_2(3-TPyP) (Soret and Q-bands at 413, 512, 545, 587 and 646 nm, compared with 420, 513, 547, 588 and 643 nm, respectively), evidencing that the redox process was localized on the ruthenium complexes. Similar behavior was observed for the protonated $H_4(3\text{-TRPyP})^{2+}$ species (Fig. 8A), except for the shift of the Q_{0-0} band at 658 to 647 nm concomitantly with the intensification and shift of the Soret band from 450 to 444 nm. Note that the spectrum of the protonated species in CH_3CN exhibits the characteristic ruthenium complex bands at 294, 365 and 496 (sh) and the porphyrin bands at 450 (Soret), 608 and 658 nm, in CH_3CN. The broad band at 496 nm, which disappeared after oxidation to the Ru(III) species, was assigned to a charge-transfer band envelope. Finally, when the potential was stepped to 1.80 V the porphyrin Soret and Q bands decreased rapidly, in both the non-protonated (Fig. 8C) and the protonated species, while the bpy $\pi \rightarrow \pi^*$ band remained unchanged, evidencing the oxidation of the porphyrin ring.

Moving to the negative side, more specifically to the −0.40 to −0.80 V range, a reversible process was observed, which caused the shift of the Soret band from 420 to 446 nm concomitantly with the increase of the absorbance at 600 nm and the decrease of the band at 514 nm (Fig. 9A). Those changes are characteristic of the reduction of the porphyrin ring to the radical anion. When the potential was shifted to −1.25 V the Soret band at 446 nm decreased while the absorbance at 800 nm was enhanced (Fig. 9B), indicating the reduction of the porphyrin ring to the dianion. The reduction of one of the bpy ligands of each peripheral ruthenium complexes to the radical anion was observed in the −1.25 to −1.50 V range, where the bpy($p\pi \rightarrow p\pi^*$) intraligand band at 297 nm decreased to about half of its initial intensity while the absorbance at 350 and 620 nm was increased (Fig. 9C). Going to more negative potentials, an intense and broad band appeared at 342 nm concomitantly with the disappearance of the bands at 297 and 441 nm, at −1.80 V, indicating the reduction of the second bpy ligand. All results are in perfect agreement with the assignment of the electrochemical processes observed in the cyclic voltammograms.

4. Conclusion

The molecular modeling calculations showed that the HOMO and LUMO of the tetraruthenated porphyrins are predominantly localized at the ruthenium complexes and porphyrin ring, respectively. Nevertheless, there are MOs with quite a high degree of orbital mixing specially in the *para*-isomer. The theoretical electronic spectra obtained by single CI ZINDO/S calculations were in fairly good agreement with the experimental data, giving a

more precise understanding of the electronic structure of the tetraruthenated porphyrins. The MOs involved in the electronic transitions showed a significant mixture of ruthenium complex and porphyrin wave functions, even in the case of the *meta*-isomer. This may explain the energy-transfer from the peripheral ruthenium complexes to the porphyrin ring, observed in the excitation spectra of both isomers in ethanol glass (77 K). Another evidence for the electronic interaction was the blue shift of the Soret and Q bands of the protonated species when the peripheral groups were oxidized to the Ru(III) complex. However, no $Ru^{II}(d\pi) \rightarrow H_4P(p\pi^*)$ charge-transfer band was found in the spectrum of the bis-protonated *meta*-isomer, in contrast with the *para*-isomer which exhibits a broad band at 704 nm. A good consistency between the theoretical and the electrochemical results was also observed, supporting the assignment and interpretation of the redox processes observed in the supramolecular porphyrins.

Acknowledgments

The authors thank the Fundação de Amparo à Pesquisa do Estado de São Paulo (FAPESP), Conselho Nacional de Desenvolvimento Científico e Tecnológico (CNPq), Rede de Nanotecnologia Molecular e Interfaces (RENAMI) and Instituto do Milênio de Materiais Complexos (IMMC) for the financial support.

References

[1] J.M. Lehn, J. Inclus. Phenom. 6 (1988) 351.
[2] J.L. Sessler, V.L. Capuano, A.K. Burrell, Inorg. Chim. Acta 204 (1993) 93.
[3] M.M.S. Paula, C.V. Franco, J. Coord. Chem. 36 (1995) 247.
[4] D. Bonifazi, M. Scholl, F.Y. Song, L. Echegoyen, G. Accorsi, N. Armaroli, F. Diederich, Angew. Chem. Int. Ed. 42 (2003) 4966.
[5] F. D'Souza, G.R. Deviprasad, M.E. Zandler, M.E. El-Khouly, M. Fujitsuka, O. Ito, J. Phys. Chem. B 106 (2002) 4952.
[6] G. Kodis, P.A. Liddell, L. de la Garza, P.C. Clausen, J.S. Lindsey, A.L. Moore, T.A. Moore, D. Gust, J. Phys. Chem. A 106 (2002) 2036.
[7] L. Flamigni, F. Barigelletti, N. Armaroli, J.P. Collin, J.P. Sauvage, J.A.G. Williams, Chem. Eur. J. 4 (1998) 1744.
[8] J. Costamagna, G. Ferraudi, J. Canales, J. Vargas, Coord. Chem. Rev. 148 (1996) 221.
[9] E. Alessio, M. Macchi, S.L. Heath, L.G. Marzilli, Inorg. Chem. 36 (1997) 5614.
[10] C.A. Hunter, R.K. Hyde, Angew. Chem. Int. Ed. 35 (1996) 1936.
[11] A.K. Burrell, D.L. Officer, D.C.W. Reid, K.Y. Wild, Angew. Chem. Int. Ed. 37 (1998) 114.
[12] H.L. Anderson, J.K.M. Sanders, J. Chem. Soc., Perkin Trans. 1 (1995) 2223.
[13] B. Steiger, F.C. Anson, Inorg. Chem. 33 (1994) 5767.
[14] E.H. Song, C.N. Shi, F.C. Anson, Langmuir 14 (1998) 4315.
[15] R.R. French, P. Holzer, M. Leuenberger, M.C. Nold, W.D. Woggon, J. Inorg. Biochem. 88 (2002) 295.
[16] J.P. Collman, L. Fu, P.C. Herrmann, X.M. Zhang, Science 275 (1997) 949.
[17] J.P. Collman, M. Rapta, M. Broring, L. Raptova, R. Schwenninger, B. Boitrel, L. Fu, M. L'Her, J. Am. Chem. Soc. 121 (1999) 1387.
[18] K. Araki, P. Losco, F.M. Engelmann, H. Winnischofer, H.E. Toma, J. Photochem. Bhotobiol. A 142 (2001) 25.
[19] K. Araki, S. Dovidauskas, H. Winnischofer, A.D.P. Alexiou, H.E. Toma, J. Electroanal. Chem. 498 (2001) 152.
[20] P.K. Sharma, S.P. de Visser, F. Ogliaro, S. Shaik, J. Am. Chem. Soc. 125 (2003) 2291.
[21] J.E. Rogers, K.A. Nguyen, D.C. Hufnagle, D.G. McLean, W.J. Su, K.M. Gossett, A.R. Burke, S.A. Vinogradov, R. Pachter, P.A. Fleitz, J. Phys. Chem. A 107 (2003) 11331.
[22] H.M. Marques, I. Cukrowski, Phys. Chem. Chem. Phys. 5 (2003) 5499.
[23] J. Linnanto, J. Korppi-Tommola, J. Comput. Chem. 25 (2004) 123.
[24] Y.T. Liao, S.Y. Ma, Acta Chim. Sinica 61 (2003) 1226.
[25] L.A. Poveda, V.R. Ferro, J.M.G. de la Vega, R.H. Gonzalez-Jonte, J. Comput. Aid. Mol. Des. 15 (2001) 183.
[26] S.H. Shi, L. Yan, Y. Yang, J. Fisher-Shaulsky, T. Thacher, J. Comput. Chem. 24 (2003) 1059.
[27] P. Arnaud, K. Zakrzewska, B. Meunier, J. Comput. Chem. 24 (2003) 797.
[28] P. Boulet, H. Chermette, C. Daul, F. Gilardoni, F. Rogemond, J. Weber, G. Zuber, J. Phys. Chem. A 105 (2001) 885.
[29] A. Rosa, G. Ricciardi, E.J. Baerends, A. Romeo, L.M. Scolaro, J. Phys. Chem. A 107 (2003) 11468.
[30] H.E. Toma, K. Araki, Coord. Chem. Rev. 196 (2000) 307.
[31] F.M. Engelmann, P. Losco, H. Winnischofer, K. Araki, H.E. Toma, J. Porphyr. Phthalocyan. 6 (2002) 33.
[32] H.E. Toma, K. Araki, A.D.P. Alexiou, S. Nikolaou, S. Dovidauskas, Coord. Chem. Rev. 219 (2001) 187.
[33] K. Araki, H. Winnischofer, H.E.B. Viana, M.M. Toyama, F.M. Engelmann, I. Mayer, A.L.B. Formiga, H.E. Toma, J. Electroanal. Chem. 562 (2004) 145.
[34] A.F. Nogueira, L.F.O. Furtado, A.L.B. Formiga, M. Nakamura, K. Araki, H.E. Toma, Inorg. Chem. 43 (2004) 396.
[35] A.F. Nogueira, A.L.B. Formiga, H. Winnischofer, M. Nakamura, F.M. Engelmann, K. Araki, H.E. Toma, Photochem. Photobiol. Sci. 3 (2004) 56.
[36] C.M.N. Azevedo, K. Araki, H.E. Toma, L. Angnes, Anal. Chim. Acta 387 (1999) 175.
[37] J.R.C. Rocha, L. Angnes, M. Bertotti, K. Araki, H.E. Toma, Anal. Chim. Acta 452 (2002) 23.
[38] N. Rea, B. Loock, D. Lexa, Inorg. Chim. Acta 312 (2001) 53.
[39] H. Winnischofer, S.D. Lima, K. Araki, H.E. Toma, Anal. Chim. Acta 480 (2003) 97.
[40] K. Kalyanasundaram, Inorg. Chem. 23 (1984) 2453.
[41] R.F. Pasternack, G.C. Centuro, P. Boyd, L.D. Hinds, P.R. Huber, L. Francesc, P. Fasella, G. Engasser, E. Gibbs, J. Am. Chem. Soc. 94 (1972) 4511.
[42] N.L. Allinger, J. Am. Chem. Soc. 99 (1977) 8127.
[43] Hypercube Inc., Gainesville, FL, USA, 2002.
[44] M.C. Zerner, G.H. Loew, R.F. Kirchner, U.T. Mueller-Westerhoff, J. Am. Chem. Soc. 102 (1980) 589.
[45] J.E. Ridley, M.C. Zerner, Theor. Chim. Acta 42 (1976) 223.
[46] J.E. Ridley, M.C. Zerner, Theor. Chim. Acta 32 (1973) 111.
[47] A.D. Bacon, M.C. Zerner, Theor. Chim. Acta 53 (1979) 21.
[48] J.J.P. Stewart, J. Comput. Chem. 10 (1989) 209.
[49] K. Kalyanasundaram, Photochemistry of Polypyridine and Porphyrin Complexes, Academic Press Inc, San Diego, 1992, p. 409.
[50] A. Juris, V. Balzani, F. Barigelletti, S. Campagna, P. Belser, A. Vonzelewsky, Coord. Chem. Rev. 84 (1988) 85.

[51] D.M. Tomazela, F.C. Gozzo, I. Mayer, F.M. Engelmann, K. Araki, H.E. Toma, M.N. Eberlin, J. Mass Spectrom. 39 (2004) 1161.
[52] P. Brandt, T. Norrby, B. Akermark, P.-O. Norrby, Inorg. Chem. 37 (1998) 4120.
[53] D.S. Eggleston, K.A. Goldsby, D.J. Hodgson, T.J. Meyer, Inorg. Chem. 24 (1985) 4573.
[54] M. Du, X.-J. Ge, H. Liu, X.-H. Bu, J. Mol. Struct. 610 (2002) 207.
[55] A. Gerli, J. Reedijk, M.T. Lakin, A.L. Speks, Inorg. Chem. 34 (1995) 1836.
[56] N.L. Allinger, X. Zhou, J. Bergsma, J. Mol. Struct. Theochem 312 (1994) 69.
[57] R.M. Badger, J. Chem. Phys. 2 (1934) 128.
[58] R.M. Badger, J. Chem. Phys. 3 (1935) 710.
[59] T.A. Halgren, J. Mol. Struct. Theochem 163 (1988) 421.
[60] B.S. Cheng, O.Q. Munro, H.M. Marques, W.R. Scheidt, J. Am. Chem. Soc. 119 (1997) 10732.
[61] V.S. Chirvony, A. van Hoek, V.A. Galievsky, I.V. Sazanovich, T.J. Schaafsma, D. Holten, J. Phys. Chem. B 104 (2000) 9909.
[62] K. Araki, M.J. Wagner, M.S. Wrighton, Langmuir 12 (1996) 5393.
[63] H. Winnischofer, F.M. Engelmann, H.E. Toma, K. Araki, H.R. Rechenberg, Inorg. Chim. Acta 338 (2002) 27.
[64] K. Araki, H.E. Toma, J. Coord. Chem. 30 (1993) 9.
[65] L.D. Sparks, C.J. Medforth, M.-S. Park, J.R. Chamberlain, M.R. Ondrias, M.O. Senge, K.M. Smith, J.A. Schelnutt, J. Am. Chem. Soc. 115 (1993) 581.
[66] K. Kalyanasundaram, M. Neumannspallart, J. Phys. Chem. 86 (1982) 5163.
[67] B.W. Durham, J.L. Walsh, C.L. Carter, T.J. Meyer, Inorg. Chem. 19 (1980) 860.